In meso crystal structure of a novel membrane-associated octaheme cytochrome *c* from the Crenarchaeon *Ignicoccus hospitalis*

Kristian Parey[1], Alistair J. Fielding[2], Matthias Sörgel[3], Reinhard Rachel[4], Harald Huber[4], Christine Ziegler [5], and Chitra Rajendran[5]

1 Department of Structural Biology, Max Planck Institute of Biophysics, Max-von-Laue-Str. 3, 60438 Frankfurt am Main, Germany,

2 School of Chemistry and the Photon Science Institute, University of Manchester, Manchester, M13 9PL, United Kingdom

3 Biogeochemistry Department, Max Planck Institute for Chemistry, Hahn-Meitner-Weg 1, 55128 Mainz, Germany

4 Department of Microbiology, University of Regensburg, Universitätsstr. 31, 93053 Regensburg, Germany

5 Department of Structural Biology, University of Regensburg, Universitätsstr. 31, 93053 Regensburg, Germany

Keywords

Archaea, Crenarchaeota, octaheme cytochrome *c*, *Ignicoccus hospitalis*, hydroxylamine oxidoreductase, nitrogen metabolism, crystal structure

Correspondence

C. Rajendran, University of Regensburg, Universitätsstr. 31, 93053 Regensburg, Germany

Fax: +49 941 9433047

Tel: +49 941 9433354

E-mail: chitra.rajendran@biologie.uni-regensburg.de

K. Parey, Max Planck Institute of Biophysics, Max-von-Laue-Str. 3, 60438 Frankfurt am Main, Germany
Fax: +49 69 63033002
Tel: +49 69 63033047
E-mail: kristian.parey@biophys.mpg.de

Abbreviations

MCC, multiheme cytochrome *c*; OCC, octaheme cytochrome *c*; HAO, hydroxylamine oxidoreductase; NeHAO, *N. europaea* HAO; KsHAO, *K. stuttgartiensis* HAO; ONR, octaheme nitrite reductases; NrfA, pentaheme nitrite reductase; MALS, multi angle light scattering; MALDI-TOF, matrix assisted laser desorption/ionization - time of flight; SDS-PAGE, sodium dodecylsulfate-polyacrylamide gel electrophoresis; EPR, electron paramagnetic resonance; NAG, N-acetylglucosamine.

Abstract

The Crenarchaeon *Ignicoccus hospitalis* lives in symbiosis with *Nanoarchaeum equitans* providing essential cell components and nutrients to its symbiont. *I. hospitalis* shows an intriguing morphology that points towards an evolutionary role in driving compartmentalization. Therefore, the bioenergetics of this archaeal host-symbiont system remains a pressing question. To date, the only electron acceptor described for *I. hospitalis*, is elemental sulfur, but the organism comprises genes that encode for enzymes involved in nitrogen metabolism, e.g., one nitrate reductase and two octaheme cytochrome *c*, Igni_0955 (IhOCC) and Igni_1359. Herein we detail functional and structural studies of the highly abundant IhOCC, including an X-ray crystal structure at 1.7 Å resolution, the first three-dimensional structure of an archaeal OCC. The trimeric IhOCC is membrane-associated and exhibits significant structural and functional differences to previously characterized homologues within the hydroxylamine oxidoreductases and octaheme cytochrome *c* nitrite reductases. The positions and spatial arrangement of the eight hemes are highly conserved, but the axial ligands of the individual hemes 3, 6 and 7 and the protein environment of the active site show significant differences. Most notably, the active site heme 4 lacks porphyrin-

tyrosine cross-links present in the HAO family. We show that IhOCC efficiently reduces nitrite and hydroxylamine, with possible relevance to detoxification or energy conservation.

Database

Structural data are available in the Protein Data Bank under the accession number 4QO5.

Introduction

Multiheme cytochromes *c* (MCCs) constitute an important class of proteins that have received considerable attention in recent decades because of their central role in global nitrogen, sulfur and iron cycling [1, 2] and its impact on the climate system [3]. The poorly-characterized clade II of the octaheme cytochromes *c* (OCC) family is closely related to both the hydroxylamine oxidoreductase (HAO) and octaheme nitrite reductases (ONR) families. In aerobic ammonium-oxidizing bacteria, the octaheme enzyme HAO is known to convert hydroxylamine (NH_2OH) to nitrite (NO_2^-), a four-electron oxidation (Equation 1) [4], whereas the ONR [5] and NrfA [6-8] enzymes convert nitrite to ammonium (NH_4^+), a six-electron reduction (Equation 2):

(Eq. 1) $NH_2OH + H_2O \rightarrow NO_2^- + 4\ e^- + 5\ H^+$

(Eq. 2) $NO_2^- + 6\ e^- + 8\ H^+ \rightarrow NH_4^+ + 2\ H_2O$

Early structural insights were obtained for the hydroxylamine oxidoreductase from the aerobic ammonium-oxidizing bacterium *Nitrosomonas europaea* (NeHAO) [9]. Each subunit of the homotrimeric NeHAO harbors eight *c*-type hemes for catalysis and electron transfer. A characteristic feature of NeHAO are two covalent bonds between the catalytic heme center of one subunit and a tyrosine residue of the adjacent subunit within the trimer [10]. Recently a HAO homologue (KsHAO) purified from the anammox bacterium *Kuenenia stuttgartiensis* was functionally and structurally characterized, which is involved in hydroxylamine detoxification [11]. NeHAO and KsHAO share important structural features including the

spatial arrangement of the heme centers and the presence of the P_{460}-type catalytic site; both use NH_2OH as their substrate, but while NeHAO forms NO_2^- as described in equation 1, KsHAO oxidizes NH_2OH predominantly to NO (Equation 3):

(Eq. 3) $NH_2OH \rightarrow NO + 3\ e^- + 3\ H^+$

The Crenarchaeon *Ignicoccus hospitalis* shows a pronounced compartmentalization unusual for a prokaryote. In has been suggested as a putative ancestor for mitochondrial evolution, a theory supported by its intimate association to the miniscule Archaeon, *Nanoarchaeum equitans* [12, 13]. Recent studies have focused on the physiological understanding of key respiratory enzymes within the different membranes of *I. hospitalis* and their bioenergetic roles.

Ignicoccus hospitalis expresses two putative OCCs, Igni_0955 and Igni_1359, that share 29% identity in a global amino acid alignment [14]. BLAST search of Igni_0955 places this protein within the HAO family of MCCs [2] but more detailed analysis [15] favors its placement within clade II of the OCC family. Despite the importance of microbial MCCs only limited structural information is available on the archaeal homologues.

This work represents the first detailed characterization of a member of the OCC family, Igni_0955 from *I. hospitalis* (IhOCC), which bears strong structural similarity to the HAOs, but with a reductive profile more similar to the ONRs. To date, all that is known about this enzyme is that it is associated both with the inner (cytoplasmic) membrane and the outer cellular membrane [14], and that it contributes to the deep red color of *I. hospitalis*. We present the IhOCC structure at 1.7 Å resolution: the first three-dimensional structure of an archaeal member of the OCC family, and the highest resolution achieved so far for an octaheme enzyme. Our structure reveals significant differences with regard to axial coordination of the individual hemes and the protein environment of the active site, compared with bacterial homologues. Our functional *in vitro* and spectroscopic studies document that IhOCC is a highly active nitrite and

hydroxylamine reductase. As such, IhOCC presents an evolutionary link between the HAO, ONR and NrfA protein families.

Results and Discussion

Molecular parameters, reactivity and spectroscopic properties of IhOCC

IhOCC was purified aerobically from *I. hospitalis* membranes by a five-step procedure to homogeneity as verified by MALDI-TOF and SDS-PAGE (Fig. 1A). Multiangle light scattering (MALS) shows that the enzyme exists as a trimer in solution (Fig. 1B) in agreement with the theoretical mass of 184.2 kDa without signal peptides and 24 *c*-type hemes. The enzyme as isolated did not oxidize hydroxylamine or hydrazine in the presence of 2.5 mM ferricyanide or 20 μM horse heart ferricytochrome *c* as electron acceptors, but catalyzed the reduction of hydroxylamine in the presence of methyl viologen (MV_{red}) as electron donor (Fig. 2A). The corresponding apparent values of k_{cat} = 91.9 ± 3.4 s^{-1}, K_m = 6.6 ± 0.6 mM and k_{cat}/K_m = 1.4 x 10^5 M^{-1} s^{-1} were obtained by fitting the data to the Michaelis-Menten equation, where k_{cat} is defined as the maximum rate of electrons transferred from MV_{red} per second and trimer. We note that NeHAO also performs this reaction but with a lower specificity constant of k_{cat}/K_m = 3.6 x 10^4 M^{-1} s^{-1} [16].

IhOCC did not react with hydrazine, nitrate, or sulfite in the presence of either reduced methyl or benzyl viologen, but exhibited a high nitrite reductase activity with benzyl viologen (BV_{red}) as electron donor with an apparent k_{cat} of 18.07 ± 0.8 s^{-1}, K_m of 0.2 ± 0.04 mM and k_{cat}/K_m = 9.0 x 10^5 M^{-1} s^{-1} (Fig. 2B), a specificity constant 100 times higher than that for the related NeHAO for the same reaction [16]. The activities for both substrates were highest at pH 7.0 (data not shown); at this pH, the specificity constant was ~6.4 times higher for nitrite than for hydroxylamine.

We did not detect formation of ammonia during the reaction of IhOCC with either nitrite or hydroxylamine as substrate by the indophenol method [17], as previously observed for NeHAO [16]. During nitrite reduction, no intermediate hydroxylamine [18] could be detected by spectrophotometric assay or capillary electrophoresis. Nitric oxide (NO) was detected during both nitrite and hydroxylamine reduction at a final concentration of 0.2% and on the order of parts per thousand, respectively. It is worth noting that NO reacts with benzyl viologen *in vitro* [19], which would act to reduce measured concentrations of intermediate NO. Formation of NO from hydroxylamine is presumably the result of a disproportionation reaction, as previously discussed for NeHAO [16, 20]. The uncatalyzed process is very slow in neutral solutions, and no measurable NO production occurred in the absence of IhOCC. Thus, the observed NO production is catalyzed *in vitro* by IhOCC under anaerobic conditions and high temperatures. For this catalytic disproportionation, two broad mechanistic possibilities exist: either two molecules of hydroxylamine react at a single active site within the course of a single catalytic cycle, which we consider unlikely due to spatial constraints, or hydroxylamine reduction at one active site is coupled via electron transfer to oxidation at another active site within the trimer. The distance between hemes of adjacent protomers (12.8 Å between Fe centers) supports the idea that this electron transfer should be possible.

The enzyme was stored in an anaerobic tent with 5% H_2 and UV/Vis spectra were recorded under anoxic conditions. The spectrum of IhOCC gave under these conditions the characteristic signature of *c*-type cytochromes in the reduced Fe(II) state with absorption maxima at 420 nm (Soret or γ-band), 524 nm (β-band) and 553 nm (α-band) (Fig. 3A) [21]. No absorption maximum around 460 nm was observed, which suggested that no P_{460} catalytic heme is present in IhOCC, as confirmed by the crystal structure (see below). Addition of excess hydroxylamine (Fig. 3A) or NO (not shown) revealed partial shifts of the γ-band to 409 nm (Soret, oxidized) and broad features of lower intensities between 500 and 600 nm, due to binding of these compounds at the heme centers. Upon addition of excess nitrite a complete

shift of the γ-peak to 409 nm and a new absorption maximum at 355 nm were observed (Fig. 3A).

The EPR spectrum (X-band, perpendicular mode, 4.3 K) of IhOCC as isolated revealed predominately resonances typical of low-spin Fe(III) centers (Fig. 3B) [22]. In particular, resonances at g = ~3.6, 1.84 and 1.56 are detected, which are similar to those reported earlier by a multifrequency EPR study of NeHAO [23] and were assigned to a pair of weakly coupled low-spin Fe(III) hemes. A resonance at g = 6 is also present, which is typical of high spin Fe(III) and likely to arise from the putative active site heme center (heme 4). Addition of an excess of nitrite, hydroxylamine and nitric oxide resulted in a reduction of the intensity of the low-spin Fe(III) features. The g = 6 resonance also changed in intensity indicating a change of environment at the catalytic heme site.

Overall structure of IhOCC

Crystals of IhOCC diffracted to 1.7 Å and data were phased by multiwavelength anomalous dispersion (MAD) using intrinsic iron atoms. Structural refinement converged to R_{work} and R_{free} values of 16.5% and 19.9%, respectively, in a resolution range of 43.7-1.7 Å (Table 1). The refined model had 96% of the non-glycine and non-proline residues in the most-favored region of a Ramachandran plot [24, 25]. In the crystalline state IhOCC revealed a homotrimeric architecture (Fig. 4A,B) as see in solution, and as reported for NeHAO [9, 10] and KsHAO [11].

The protein is characterized by highly charged surface areas (Fig. 4C,D), with the bottom carrying mainly positive charges. The intra-trimeric contacts are mediated by a total of 26 hydrogen bonds and 6 salt bridges; no covalent bonds are present. Comparison of the overall structures of IhOCC and NeHAO (4FAS [10]) reveals a root-mean-square deviation (r.m.s.d.) of 3.1 Å for 358 equivalent C^{α} positions, and an overall sequence identity of 23% (Fig. S1). The

sequence identity between IhOCC and KsHAO (kustc1061, 4N4J; [11]) is 21% and these structures superpose with an r.m.s.d. of 2.6 Å for 338 equivalent Cα positions. The first 28 amino acids of IhOCC were not resolved, most likely due to N-terminal processing of the predicted signal sequence. A free cysteine (Cys179) was detected, which is very rare in *c*-cytochromes except for the catalytic sites of octaheme tetrathionate reductases (OTR) [26] and ONR [27].

Heme arrangement and axial ligation

A search for the classical Cys-x-x-Cys-His binding motif within the IhOCC amino acid sequence identified a total of eight putative *c*-type heme centers, which was confirmed by the crystal structure. The distances between adjacent heme iron atoms – ranging from 9.2 to 12.0 Å - should allow for efficient electron transfer [28]. The heme centers were grouped into four different clusters (Fig. 5). In contrast to NeHAO and KsHAO, which both show overall bis-histidine axial coordination at all hemes, in IhOCC hemes 1, 2, 5, and 8 have bis-histidinyl ligands, while the iron atoms of hemes 3 and 7 are His-Met coordinated, and the iron atom of heme 6 is coordinated by His-Lys. Heme 4, the putative active site, is axially coordinated by His-H_2O (Fig. 6A-H and Table 2).

In the diheme cluster I (Fig. 6A,B and Table 2), hemes 3 and 5 show a parallel arrangement. Heme 5 has axial ligands His247 and His334, and is linked by Cys243 and Cys246 to the peptide backbone, with hydrophobic residues in close proximity to the porphyrin moiety (Fig. 6B). In heme 3, the iron is axially coordinated by His142 and Met71 (Fig. 6A and Table 2). This His-Met coordination is absent in all known OCC and HAO homologues (Fig. S2) except in *Ignicoccus islandicus*. Again, heme 3 is embedded in a pronounced hydrophobic environment.

Diheme cluster II is the most conserved and shows strong similarities to the same cluster found in NeHAO and KsHAO. Heme 1 is covalently bonded by Cys51 and Cys54, and the Fe ligated by His55 and His124, with eight residues forming the hydrophobic pocket (Fig. 6C and Table 2). Heme 2 is held in place by Cys107, Cys110, His111 and His250, with four residues creating a hydrophobic environment (Fig. 6D and Table 2).

The triheme cluster (Fig. 6E, F, G and Table 2) harbors the putative active site heme 4 and hemes 6 and 7. Hemes 6 and 7 are surrounded as well by hydrophobic residues (Fig. 6F, G and Table 2). Interestingly, heme 6 is axially coordinated by Lys154 and His267, a coordination which is described here for the first time for a member of the MCC superfamily. This combination is conserved for OCCs from Archaea and anammox bacteria whereas in *Desulfuromonas acetoxidans* lysine is replaced by methionine (Fig. S2). Arg343, Pro354, His351 and His359 form a tight network of hydrogen bonds with several water molecules and the propionates from hemes 4 and 6, which acts to stabilize the porphyrin moieties (Fig. 7A). These interactions between hemes 4 and 6 are different in NeHAO where a proline (Pro202) is located near the corresponding guanidinium group of Arg343 and imidazole nitrogen of His359, which is inserted between the propionate residues of P_{460} and heme 6. Heme 7 shows a His-Met axial coordination with a distance of 2.4 Å from Met514 to the iron. A similar coordination is present for related members in the characterized group (Fig. S2). The single heme 8 is axially coordinated by His283 and His439 (Fig. 6H and Table 2). Five residues are forming the hydrophobic milieu of this heme.

Active site

Unlike NeHAO, which comprises only one channel, IhOCC contains a branched channel that connects heme 4 in each subunit with the surface of IhOCC (Fig. 7B). One exhibits a pronounced positive electrostatic surface potential, presumably to attract a negatively charged

substrate such as nitrite (Fig. 4C and 7B). The other one is negatively charged, which we annotate as an exit channel and where the final products are presumably released.

Unlike all other HAOs, IhOCC does not exhibit an optical absorption around 460 nm characteristic of a P_{460} heme center in the reduced Fe(II) state (Fig. 3A). P_{460} heme center contain a conserved Tyr that is replaced by phenylalanine in IhOCC (Phe522) (Figs. 6E and 7A, Fig. S2). Typical intersubunit cross-links to the catalytic heme formed by phenylalanine were observed in NeHAO and KsHAO [9-11]. In these bacterial homologues, Tyr is proposed to increase the stability of an Fe(III)NO intermediate by a connection of its aromatic ring with the P_{460} porphyrin moiety and the abstraction of two protons and two electrons [29].

The iron atom of heme 4 is axially coordinated by His199, at a Fe-N distance of 2.3 Å and as an water oxygen interpreted, which is hydrogen bonded to OD1 of Asp271 and the iron each with a distance of 2.5 Å (Figs. 6E and 7A). Notably, the catalytically relevant residues histidine and tyrosine found in NrfA (His282 and Tyr217) [30], ONR (His361 and Tyr303) [5] and NeHAO (His268 and Tyr358) [9, 10], are replaced by valine (Val272) and phenylalanine (Phe345) suggesting that catalysis by IhOCC may proceed via a different mechanism than in these homologues. Exchange of active-site tyrosine to phenylalanine in NrfA from *W. succinogenes* led to a nearly complete loss of nitrite reductase activity [31] and replacement of the heme-coordinating lysine to histidine decreased the activity to 35% [32].

In NrfA from *W. succinogenes*, protons needed for the reduction of nitrite to ammonia (Equation 2) are thought to be delivered by Arg114 and His277 leading to energetically feasible, low-barrier protonation reactions [33]. In IhOCC, the protons for the reaction are most likely delivered via the Grotthuss mechanism by solvent molecules [34], present in a funnel appearing from the top running through the center of the trimer (Fig. 4). The Protons appeared to be first transferred to Asp518. In such a scenario, the side chain of Asp518 would flip toward the active site and displace the protons to Asp271. The electrons for IhOCC could be provided by an

unknown interaction partner with heme 1 of diheme cluster II as entry point and from the adjacent subunit (Fig. 7B).

One striking feature of the IhOCC structure is the hydrophobic environment of heme 4. (Fig. 6E and Table 2). Such a hydrophobic environment would strongly disfavor that the product of the reduction of nitrite or hydroxylamine is the positively charged ammonium ion NH_4^+, but more likely the neutral NH_3. Here, we demonstrate the formation of the gaseous compound NO from both substrates in low amounts. The generation of other neutral gases from nitrite, such as N_2 or N_2O, is rather unlikely but cannot be excluded. In the case of hydroxylamine as substrate, the gene product Igni_0960, annotated as a hydroxylamine reductase based on sequence identity, might show a higher affinity to hydroxylamine and is therefore the preferred enzyme for this specific reaction. Further investigations will be needed to elucidate this point.

Ca^{2+} and N-acetylglucosamine (NAG)

Each protomer within the trimer shows the presence of a tightly bound Ca^{2+} ion in the proximity of heme 4 (Figs. 4A and 5, Fig. S3), which is not present in the structures of NeHAO and KsHAO. The Ca^{2+}-Fe has a distance of 20.9 Å, which is almost double compared to other NrfAs and ONRs [27, 30, 35, 36], where in the latter a second Ca^{2+} ion is located near heme 3 and 4. The Ca^{2+} ion in IhOCC is bound with a coordination number of 7 and is located in the C-terminal part of the enzyme. This type of coordination is formed by four oxygens of the carboxy groups from Asp490, Glu491 and Glu494, two peptide carbonyl oxygens of His479 and Thr487, and one water molecule (HOH59) (Fig. S3). In NrfAs, the Ca^{2+} ion is octahedrally coordinated by the carboxy group of a glutamate in a bidentate manner and by a glutamine, two carbonyl oxygens of a tyrosine and lysine residue, and two water molecules. All calcium-coordinating residues are strictly conserved for NrfAs. In OCCs, only Asp490, Glu491 and Glu494 are conserved, whereas the latter also can be found in CsHAO and NeHAO (Fig. S2).

A NAG molecule, a monosaccharide derivative of glucose, could be modeled into the electron density (Figs. 4A, 5 and 6E, Fig. S4), interacting with the amine group of Asp172. An unidentified density, emerging from the NAG might be attributed to a lipid moiety. One possibility would be monoglycosyl-archaeol, which is the main lipid in the outer cellular membrane of *I. hospitalis* and could have been co-purified from the membranes [37]. The presence of this lipid at this specific site points towards a potential entry site for electrons via the membrane, delivered by respiratory chain complexes (Fig. 7B) [14].

Evolutionary analysis and conservation of IhOCC

Our molecular, functional and structural analyses in this present study showed that IhOCC belongs to clade II of the OCC family suggesting an evolutionary relationship and a link between HAO, ONR and NrfA. Thus, IhOCC represents an intermediate not only in a phylogenetic sense but also in terms of structural and functional characteristics, with a high structural similarity to the HAO family but reductive properties more similar to ONR.

In addition to the conservation of the functional residues and secondary structure, there is a high sequence identity of 45% between the archaeal IhOCC and bacterial KsOCC (kuste2435) from *K. stuttgartiensis* (Fig. S2). Similar to IhOCC, the cross-linked tyrosine in the C-terminus is absent, which is thought to facilitate reductive catalysis [38]. Beside kuste2435 nine different paralogues are encoded in the *K. stuttgartiensis* genome, suggesting an important physiological role for these proteins in the anammox metabolism.

This is not the only similarity between *Ignicoccus* species and anammox bacteria. Planctomycetes comprises proteins as a major outer membrane constituen [39], a feature that is observed in the outer cell membrane of *Ignicoccus,* too. The outer cell wall is densely packed with membrane-bound and membrane-embedded proteins. Planctomycetes also show compartmentalized cell architecture similar to *Ignicoccus* [40]. In Planctomycetes, intracellular membranes divide the cytoplasm into different compartments, while in *Ignicoccus* the

intermembrane compartment and the cytoplasm represent two different compartments, with the cytoplasm of the associated *Nanoarchaeum* representing a third compartment.

Can IhOCC work also as a sulfite reducer?

Our structural and activity data indicate that NO_2^- is the preferred substrate of IhOCC. Hydroxylamine is also a substrate but is converted with a significantly lower affinity. MCC enzymes, such as pentaheme NrfAs, not only transform NO_2^- to NH_4^+, which is the key reaction in respiratory nitrite ammonification, but also converts NO, NH_2OH, H_2O_2, and SO_3^{2-}, although with lower activity [31]. Additionally, *S. deleyianum* assembles NrfA at high levels when grown on elemental sulfur, indicating a physiological role for this protein´s reaction [41]. Although *I. hospitalis* has been reported to be a strict sulfur-reducing organism, the membrane-associated octaheme enzyme IhOCC did not convert sulfur compounds, such as sulfite and sulfide, under our experimental conditions [42]. The possibility remains that IhOOC1 could also reduce sulfur compounds *in vivo*, i.e., at high pressure and temperature above 80 ˚C.

Detoxification or utilization of nitrite: a putative role of IhOCC in *I. hospitalis*

In context of its nitrite reductase activity, possible roles of IhOCC are detoxification of the intermediate nitrite or for respiratory energy conservation. In methanotrophic bacteria a crucial role for HAO-like proteins for nitrogen oxide metabolism and detoxification was suggested, which could either oxidize hydroxylamine to nitrite or NO or alternatively reduce nitrite to NO [43, 44]. Moreover, a putative role of IhOCC in the respiratory chain of *I. hospitalis* will become important under growth conditions where no sulfur is available. A pathway of respiratory nitrite reduction during the anaerobic growth of *I. hospitalis* when nitrate or nitrite is available as an electron acceptor is plausible and supported by our structure function study. The presence of genes encoding for proteins/enzymes involved in nitrogen energy conservation is a strong

argument taken into account that *I. hospitalis* comprises the smallest genome of all independent organisms discovered so far, and assuming that all genes in the genome being essential [45].

.

Experimental procedures

Cultivation of *I. hospitalis*

Type strain *I. hospitalis* KIN4/I^T (DSM 18386) was obtained from our culture collection at the Institute of Microbiology and Archaeal Center, University of Regensburg. Cells were grown routinely in 1/2 SME-*Ignicoccus* medium at 90 °C as described previously [13, 42] with H_2-CO_2 (80/20 [vol/vol], 250 kPa) as gas phase, thereby using hydrogen as an electron donor and elemental sulfur as an electron acceptor. Batch cultures were grown in 300-liter enamel-protected fermenters at 90 °C, pH 5.5 to 6.0. To reach final cell densities of ~10^8 cells ml^{-1}, a flow rate of 60 liters of the gas mixture $H_2/N_2/CO_2$ (15:65:20 [vol/vol/vol]) min^{-1} was applied. The cells were harvested by centrifugation (Padberg, Germany), shock-frozen in liquid nitrogen, and stored at -80 °C until use.

Purification of IhOCC from *I. hospitalis*

All protein concentrations were determined with a BCA Protein Assay Kit (Thermo Scientific, Germany) and all purification steps were performed aerobically. 20 g cells were thawed, suspended in hypotonic buffer A (5 mM KH_2PO_4, 1 mM EDTA-Na_2, 1.4 mM $MgSO_4$, 1 mM PMSF, pH 4.4) and disrupted by a glass potter homogenizer. Remaining cells and cell debris were removed by centrifugation (5,000 x *g* at 4 °C for 20 min), followed by ultracentrifugation (Beckman Optima XPN-100 45 Ti rotor, 138,000 x *g*, 2 h, 4 °C). The pellet was suspended in 25 mM MOPS/NaOH pH 7.2, 50 mM NaCl and 3 mM $MgCl_2$ (buffer B). The membranes were solubilized in dodecyl maltoside (DDM) (Glycon, Germany) with a final concentration of 1.0% for 1 h at room temperature by applying the ratio 4 mg detergent to 1 mg protein. Insoluble

components were removed by ultracentrifugation (Beckman Optima XPN-100, 45 Ti rotor, 138,000 x *g*, 30 min, 4 °C) and the supernatant was applied to a chromatographic step using a HiTrap Q FF column (GE Healthcare, USA). The flow through was collected and loaded on a HiTrap SP FF column (GE Healthcare, USA). The flow through was concentrated by ultrafiltration (Amicon Ultra-4, 100 kDa cut-off; Millipore, Germany), adjusted to a protein concentration of 10 mg/ml and loaded onto a Superdex 200 pg HiLoad 16/600 gel filtration column (GE Healthcare, USA) equilibrated with buffer B supplemented with 0.05% DDM. Proteins eluted in four peaks with the majority of the heme-containing proteins eluting within the second and third peaks as determinated by UV/Vis spectroscopy. These fractions were pooled, concentrated to approximately 10 mg/ml (Amicon Ultra-4, 100 kDa cut-off; Millipore, Germany) and dialyzed against a buffer containing 10 mM K-phosphate pH 7.0 and 0.05% DDM (buffer C). The protein solution was applied to a Hydroxyapatite type II 0.2 µm column (Bio-Rad, Germany) and eluted in a stepwise K-phosphate gradient (20 mM, 70 mM, 140 mM and 1 M) at 70 mM K-phosphate pH 7.0. The combined fractions were concentrated by ultrafiltration, adjusted to a protein concentration of 10 mg/ml and loaded onto a Superdex 200 10/300 GL gel filtration column (GE Healthcare, USA) equilibrated with 20 mM Tris-HCl pH 7.0 (buffer D). Eluted protein was concentrated to 6 mg/ml and stored at 4 °C for further use.

Enzyme assays and end product analysis

Enzyme activities were routinely determined at 80 °C under strictly anaerobic conditions. Protein was quantified with the Bio-Rad protein assay using ovalbumin as standard. 1.5 ml anoxic SUPRASIL UV cuvettes from Hellma containing 1.0 ml assay mixture were sealed by boiled and autoclaved butyl rubber stoppers from Deutsch & Naumann. Components were added anoxically by Hamilton syringes (Bonaduz, Switzerland). The standard mixture contained 50 mM K-phosphate pH 7.0, 0.25 mM sodium dithionite and 1.0 mM methyl

viologen or benzyl viologen. The reaction was started with addition of 7.5 µM - 10 mM hydroxylamine or 2.5 µM - 2 mM nitrite, respectively, and 1.25 µg enzyme after a 1-min prior incubation at 80 °C. The reaction was monitored spectrophotometrically at 578 nm (ϵ = 8.6 mM^{-1} cm^{-1}) for benzyl viologen and 600 nm (ϵ = 13.7 mM^{-1} cm^{-1}) for methyl viologen. Primary plots of initial rate against substrate concentration fit to the Michealis-Menten equation were created and analyzed by non-linear regression using SigmaPlot (version 12.5; Systat Software Inc).

Nitric oxide was quantified by a chemiluminescence gas analyzer (CLD 790 SR, ECOPHYSICS, Switzerland, limit of detection (LOD): $LOD_{NO} \approx 10$ ppt). The measurement frequency was 8 Hz allowing for high time resolution. The headspace of the sample vials was flushed with nitrogen ($1.5 \cdot 10^{-5}$ m^3 s^{-1}), further diluted with nitrogen ($1.4 \cdot 10^{-5}$ m^3 s^{-1}) outside of the vial and supplied to the analyzer.

Spectroscopy

The enzyme for UV/Vis measurements was stored under anoxic conditions for several days and incubated with either 20 mM nitrite or hydroxylamine up to 15 hours. UV/Vis spectra (300-750 nm) were recorded with a Cary 50 spectrometer (Varian, Germany) in quartz cells (5.0 mm path length) at 22 °C.

Samples for EPR measurements (as isolated and 2 mM substrate each) were transferred to calibrated 3.0 mm quartz tubes and frozen in liquid nitrogen. Continuous-wave EPR spectra were recorded at 9.4 GHz (X-band) on a Bruker EMX spectrometer with a Super-high-Q rectangular cavity and an Oxford ESR-900 liquid helium cryostat. The operating conditions were: 4.3 K, 4.0 G modulation amplitude at 100 kHz, and microwave power of 0.3 mW. Spectra were recorded using 20 scans and plotted using OriginPro (version 8.5.1; OriginLab).

Light scattering

Oligomerisation of IhOCC was analyzed by MALS (multi angle light scattering) using Viscotek TDA 305 from Malvern Instruments, UK. Approximately 100 µl of the protein sample with a concentration of 2 mg ml^{-1} was injected into equilibrated and calibrated Viscotek TDA 305 through an ÄKTA system (GE Healthcare, USA). The molecular weight of the protein was determined using the Conjugate method from Malvern Instruments.

Crystallization and X-ray data collection

Initial crystals were obtained at 18 °C with the hanging-drop method using the Hampton PEGRx HT sparse-matrix screening setup. Further optimization led to a drop content of 1µl enzyme solution (6 mg ml^{-1}) and 1 µl reservoir solution (100 mM Tris-HCl pH 8.0, 100 mM sodium malonate pH 8.0 and 28% PEG 1000). Crystals diffracted to 7 Å and further optimization was performed *in meso.* The mesophase was prepared by mixing monoolein as host lipid and protein using the two syringe method as previously described [46]. The *meso* phase with protein was prepared as a 3/2 by volume mix of lipid and protein solution and dispensed in a 96-well crystallization plate using a mosquito LCP from TTP Labtech, UK. Crystallization trials were performed with 50 nl protein/lipid dispersion and 1 µl precipitant solution at 20 °C.

Crystals *in meso* were grown in the space group R 3 2 :H with unit cell parameters of a=136.44 Å, b=136.44 Å, c=214.9 Å, α=β=90° and γ=120° with one subunit in the asymmetric unit (V_M = 3.22 $Å^3Da^{-1}$, solvent content 61.8%). *In meso* crystals were tiny and diffracted to a resolution of 1.1 Å. Data from several crystals were merged and scaled to get sufficient anomalous signal and completeness. Merged data with a final resolution of 1.7 Å were used for structure solution. The data were collected at 100 K at the beamline PXI of the Swiss Light Source (SLS) at the Paul Scherrer Institute in Villigen, Switzerland and processed using the XDS program suite (Table 1) [47].

Phase determination and refinement

The irons of hemes *c* were found using SHELXD [48]. Model building was performed by the program COOT [49]. Refinement was brought to convergence using REFMAC and PHENIX [50, 51]. The refinement statistics are given in Table S1. The quality of the model was checked with PROCHECK [24] and MolProbity [25]. Figures were generated with PYMOL (The PyMOL Molecular Graphics System, Schrödinger, LLC.).

Acknowledgments

The authors wish to thank T. Hader and K. Eichinger for mass cultivation of cells and the staff of the beamline PXI of the Swiss Light Source (SLS) at the Paul Scherrer Institute in Villigen, Switzerland. A.J.F. thanks Bruker for sponsorship and the EPSRC National (UK) EPR Research Facility & Service. We thank Klaus Tiefenbach for figure illustration and Bonnie Murphy for critical reading of the manuscript. This work was supported by the Deutsche Forschungsgemeinschaft Grant HU703/2-2 (to H.H. and R.R.).

Author contributions

K.P., R.R., H.H., C.Z., and C.R. designed the study, interpreted the data and wrote the paper. K.P. purified, crystallized and characterized IhOCC protein. C.R. performed MALS, crystallized IhOCC protein *in meso* and determined its X-ray structure. A.J.F. performed EPR studies and M.S. the end product analysis.

Notes

The authors declare no competing financial interest.

References

1. Simon, J., Kern, M., Hermann, B., Einsle, O. & Butt, J. N. (2011) Physiological function and catalytic versatility of bacterial multihaem cytochromes *c* involved in nitrogen and sulfur cycling, *Biochem Soc Trans.* **39**, 1864-70.

2. Simon, J. & Klotz, M. G. (2013) Diversity and evolution of bioenergetic systems involved in microbial nitrogen compound transformations, *Biochim Biophys Acta.* **1827**, 114-35.

3. Stevenson, F. J. & Cole, M. A. (1999) *Cycles of soils: carbon, nitrogen, phosphorus, sulfur, micronutrients*, John Wiley & Sons.

4. Hooper, A. B. & Nason, A. (1965) Characterization of hydroxylamine-cytochrome *c* reductase from the chemoautotrophs *Nitrosomonas europaea* and *Nitrosocystis oceanus*, *J Biol Chem.* **240**, 4044-57.

5. Tikhonova, T., Tikhonov, A., Trofimov, A., Polyakov, K., Boyko, K., Cherkashin, E., Rakitina, T., Sorokin, D. & Popov, V. (2012) Comparative structural and functional analysis of two octaheme nitrite reductases from closely related *Thioalkalivibrio* species, *The FEBS journal.* **279**, 4052-61.

6. Bamford, V. A., Angove, H. C., Seward, H. E., Thomson, A. J., Cole, J. A., Butt, J. N., Hemmings, A. M. & Richardson, D. J. (2002) Structure and spectroscopy of the periplasmic cytochrome *c* nitrite reductase from *Escherichia coli*, *Biochemistry.* **41**, 2921-31.

7. Pereira, I. C., Abreu, I. A., Xavier, A. V., LeGall, J. & Teixeira, M. (1996) Nitrite reductase from *Desulfovibrio desulfuricans* (ATCC 27774)--a heterooligomer heme protein with sulfite reductase activity, *Biochemical and biophysical research communications.* **224**, 611-8.

8. Schumacher, W., Hole, U. & Kroneck, P. M. (1994) Ammonia-forming cytochrome *c* nitrite reductase from *Sulfurospirillum deleyianum* is a tetraheme protein: new aspects of the molecular composition and spectroscopic properties, *Biochemical and biophysical research communications.* **205**, 911-6.

9. Igarashi, N., Moriyama, H., Fujiwara, T., Fukumori, Y. & Tanaka, N. (1997) The 2.8 Å structure of hydroxylamine oxidoreductase from a nitrifying chemoautotrophic bacterium, *Nitrosomonas europaea*, *Nature structural biology.* **4**, 276-84.

10. Cedervall, P., Hooper, A. B. & Wilmot, C. M. (2013) Structural studies of hydroxylamine oxidoreductase reveal a unique heme cofactor and a previously unidentified interaction partner, *Biochemistry.* **52**, 6211-8.

11. Maalcke, W. J., Dietl, A., Marritt, S. J., Butt, J. N., Jetten, M. S., Keltjens, J. T., Barends, T. R. & Kartal, B. (2014) Structural basis of biological NO generation by octaheme oxidoreductases, *J Biol Chem.* **289**, 1228-42.

12. Huber, H., Küper, U., Daxer, S. & Rachel, R. (2012) The unusual cell biology of the hyperthermophilic Crenarchaeon *Ignicoccus hospitalis*, *Antonie Van Leeuwenhoek.* **102**, 203-19.

13. Huber, H., Hohn, M. J., Rachel, R., Fuchs, T., Wimmer, V. C. & Stetter, K. O. (2002) A new phylum of Archaea represented by a nanosized hyperthermophilic symbiont, *Nature.* **417**, 63-7.

14. Naß, B., Poll, U., Langer, J. D., Kreuter, L., Küper, U., Flechsler, J., Heimerl, T., Rachel, R., Huber, H. & Kletzin, A. (2014) Three multihaem cytochromes *c* from the hyperthermophilic archaeon *Ignicoccus hospitalis*: purification, properties and localization, *Microbiology.* **160**, 1278-89.

15. Klotz, M. G., Schmid, M. C., Strous, M., op den Camp, H. J., Jetten, M. S. & Hooper, A. B. (2008) Evolution of an octahaem cytochrome *c* protein family that is key to aerobic and anaerobic ammonia oxidation by bacteria, *Environmental microbiology.* **10**, 3150-63.

16. Kostera, J., McGarry, J. & Pacheco, A. A. (2010) Enzymatic interconversion of ammonia and nitrite: the right tool for the job, *Biochemistry.* **49**, 8546-53.

17. Boltz, D. F. & Taras, M. J. (1978) Nitrogen in *Colorimetric Determination of Nonmetals* (Boltz, D. F. & Howell, J. A., eds) pp. 197-251, John Wiley & Sons Inc., New York.

18. Einsle, O., Messerschmidt, A., Huber, R., Kroneck, P. M. & Neese, F. (2002) Mechanism of the six-electron reduction of nitrite to ammonia by cytochrome *c* nitrite reductase, *J Am Chem Soc.* **124**, 11737-45.

19. Irisa, T., Hira, D., Furukawa, K. & Fujii, T. (2014) Reduction of nitric oxide catalyzed by hydroxylamine oxidoreductase from an anammox bacterium, *Journal of bioscience and bioengineering.* **118**, 616-21.

20. Pacheco, A. A., McGarry, J., Kostera, J. & Corona, A. (2011) Techniques for investigating hydroxylamine disproportionation by hydroxylamine oxidoreductases, *Methods in enzymology.* **486**, 447-63.

21. Hooper, A. B. & Nason, A. (1965) Characterization of hydroxylamine-cytochrome *c* reductase from the chemoautotrophs *Nitrosomonas europaea* and *Nitrosocystis oceanus*, *The Journal of biological chemistry.* **240**, 4044-57.

22. Lipscomb, J. D. & Hooper, A. B. (1982) Resolution of multiple heme centers of hydroxylamine oxidoreductase from *Nitrosomonas*. 1. Electron paramagnetic resonance spectroscopy, *Biochemistry.* **21**, 3965-72.

23. Hendrich, M. P., Logan, M., Andersson, K. K., Arciero, D. M., Lipscomb, J. D. & Hooper, A. B. (1994) The Active-Site of Hydroxylamine Oxidoreductase from *Nitrosomonas* - Evidence for a New Metal Cluster in Enzymes, *J Am Chem Soc.* **116**, 11961-11968.

24. Laskowski, R. A., MacArthur, M. W., Moss, D. S. & Thornton, J. M. (1993) PROCHECK: a program to check the stereochemical quality of protein structures, *J Appl Cryst* **26**, 283-291.

25. Chen, V. B., Arendall, W. B., 3rd, Headd, J. J., Keedy, D. A., Immormino, R. M., Kapral, G. J., Murray, L. W., Richardson, J. S. & Richardson, D. C. (2010) MolProbity: all-atom structure validation for macromolecular crystallography, *Acta crystallographica Section D, Biological crystallography.* **66**, 12-21.

26. Mowat, C. G., Rothery, E., Miles, C. S., McIver, L., Doherty, M. K., Drewette, K., Taylor, P., Walkinshaw, M. D., Chapman, S. K. & Reid, G. A. (2004) Octaheme tetrathionate reductase is a respiratory enzyme with novel heme ligation, *Nat Struct Mol Biol.* **11**, 1023-4.

27. Polyakov, K. M., Boyko, K. M., Tikhonova, T. V., Slutsky, A., Antipov, A. N., Zvyagilskaya, R. A., Popov, A. N., Bourenkov, G. P., Lamzin, V. S. & Popov, V. O. (2009) High-resolution structural analysis of a novel octaheme cytochrome *c* nitrite reductase from the haloalkaliphilic bacterium *Thioalkalivibrio nitratireducens*, *Journal of molecular biology.* **389**, 846-62.

28. Page, C. C., Moser, C. C. & Dutton, P. L. (2003) Mechanism for electron transfer within and between proteins, *Current opinion in chemical biology.* **7**, 551-6.

29. Fernandez, M. L., Estrin, D. A. & Bari, S. E. (2008) Theoretical insight into the hydroxylamine oxidoreductase mechanism, *J Inorg Biochem.* **102**, 1523-30.

30. Einsle, O., Messerschmidt, A., Stach, P., Bourenkov, G. P., Bartunik, H. D., Huber, R. & Kroneck, P. M. (1999) Structure of cytochrome *c* nitrite reductase, *Nature.* **400**, 476-80.

31. Lukat, P., Rudolf, M., Stach, P., Messerschmidt, A., Kroneck, P. M., Simon, J. & Einsle, O. (2008) Binding and reduction of sulfite by cytochrome *c* nitrite reductase, *Biochemistry.* **47**, 2080-6.

32. Rudolf, M. (2004) *Cytochrome c Nitrite Reductase : further Investigations of the Multiheme Enzyme by X-Ray Crystallography, Site-Directed Mutagenesis, and EPR Spectroscopy*, University of Constance.

33. Bykov, D. & Neese, F. (2011) Substrate binding and activation in the active site of cytochrome *c* nitrite reductase: a density functional study, *J Biol Inorg Chem.* **16**, 417-30.

34. de Grotthuss, C. J. T. (1806) Sur la decomposition de l'eau et des corps qu'elle tient en dissolution a l'aide de l'electricite galvanique., *Ann Chim.* **58**, 54-73.

35. Cunha, C. A., Macieira, S., Dias, J. M., Almeida, G., Goncalves, L. L., Costa, C., Lampreia, J., Huber, R., Moura, J. J., Moura, I. & Romao, M. J. (2003) Cytochrome *c* nitrite reductase

from *Desulfovibrio desulfuricans* ATCC 27774. The relevance of the two calcium sites in the structure of the catalytic subunit (NrfA), *J Biol Chem.* **278**, 17455-65.

36. Einsle, O., Stach, P., Messerschmidt, A., Simon, J., Kroger, A., Huber, R. & Kroneck, P. M. (2000) Cytochrome *c* nitrite reductase from *Wolinella succinogenes*. Structure at 1.6 Å resolution, inhibitor binding, and heme-packing motifs, *J Biol Chem.* **275**, 39608-16.

37. Jahn, U., Summons, R., Sturt, H., Grosjean, E. & Huber, H. (2004) Composition of the lipids of *Nanoarchaeum equitans* and their origin from its host *Ignicoccus* sp. strain KIN4/I, *Archives of microbiology.* **182**, 404-13.

38. Kartal, B., de Almeida, N. M., Maalcke, W. J., Op den Camp, H. J., Jetten, M. S. & Keltjens, J. T. (2013) How to make a living from anaerobic ammonium oxidation, *FEMS Microbiol Rev.* **37**, 428-61.

39. Fuerst, J. A., Webb, R. I., Van Niftrik, L., Jetten, M. S. & Strous, M. (2006) Complex intracellular structures in prokaryotes, Chapter 10: Anammoxosomes of anaerobic ammonium-oxidizing planctomycetes in *Microbiology Monographs* (Shiveley, J. M., ed) pp. 259–608, Springer-Verlag, Berlin and Heidelberg.

40. van Niftrik, L. & Jetten, M. S. (2012) Anaerobic ammonium-oxidizing bacteria: unique microorganisms with exceptional properties, *Microbiology and molecular biology reviews : MMBR.* **76**, 585-96.

41. Zophel, A., Kennedy, M. C., Beinert, H. & Kroneck, P. M. (1991) Investigations on microbial sulfur respiration. Isolation, purification, and characterization of cellular components from Spirillum 5175, *Eur J Biochem.* **195**, 849-56.

42. Paper, W., Jahn, U., Hohn, M. J., Kronner, M., Nather, D. J., Burghardt, T., Rachel, R., Stetter, K. O. & Huber, H. (2007) *Ignicoccus hospitalis* sp. nov., the host of '*Nanoarchaeum equitans*', *International journal of systematic and evolutionary microbiology.* **57**, 803-8.

43. Campbell, M. A., Nyerges, G., Kozlowski, J. A., Poret-Peterson, A. T., Stein, L. Y. & Klotz, M. G. (2011) Model of the molecular basis for hydroxylamine oxidation and nitrous oxide production in methanotrophic bacteria, *FEMS Microbiol Lett.* **322**, 82-9.

44. Poret-Peterson, A. T., Graham, J. E., Gulledge, J. & Klotz, M. G. (2008) Transcription of nitrification genes by the methane-oxidizing bacterium, *Methylococcus capsulatus* strain Bath, *ISME J.* **2**, 1213-20.

45. Giannone, R. J., Huber, H., Karpinets, T., Heimerl, T., Küper, U., Rachel, R., Keller, M., Hettich, R. L. & Podar, M. (2011) Proteomic characterization of cellular and molecular processes that enable the *Nanoarchaeum equitans-Ignicoccus hospitalis* relationship, *PLoS One.* **6**, e22942.

46. Caffrey, M. & Cherezov, V. (2009) Crystallizing membrane proteins using lipidic mesophases, *Nat Protoc.* **4**, 706-31.

47. Kabsch, W. (1993) Automatic processing of rotation diffraction data from crystals of initially unknown symmetry and cell constants., *J Appl Cryst.* **26**, 795-800.

48. Sheldrick, G. M. (2010) Experimental phasing with SHELXC/D/E: combining chain tracing with density modification, *Acta crystallographica Section D, Biological crystallography.* **66**, 479-85.

49. Emsley, P., Lohkamp, B., Scott, W. G. & Cowtan, K. (2010) Features and development of Coot, *Acta crystallographica Section D, Biological crystallography.* **66**, 486-501.

50. Murshudov, G. N., Vagin, A. A. & Dodson, E. J. (1997) Refinement of macromolecular structures by the maximum-likelihood method, *Acta crystallographica Section D, Biological crystallography.* **53**, 240-55.

51. Afonine, P. V., Grosse-Kunstleve, R. W., Echols, N., Headd, J. J., Moriarty, N. W., Mustyakimov, M., Terwilliger, T. C., Urzhumtsev, A., Zwart, P. H. & Adams, P. D. (2012) Towards automated crystallographic structure refinement with phenix.refine, *Acta crystallographica Section D, Biological crystallography.* **68**, 352-67.

52. Baker, N. A., Sept, D., Joseph, S., Holst, M. J. & McCammon, J. A. (2001) Electrostatics of nanosystems: application to microtubules and the ribosome, *Proc Natl Acad Sci U S A.* **98**, 10037-41.

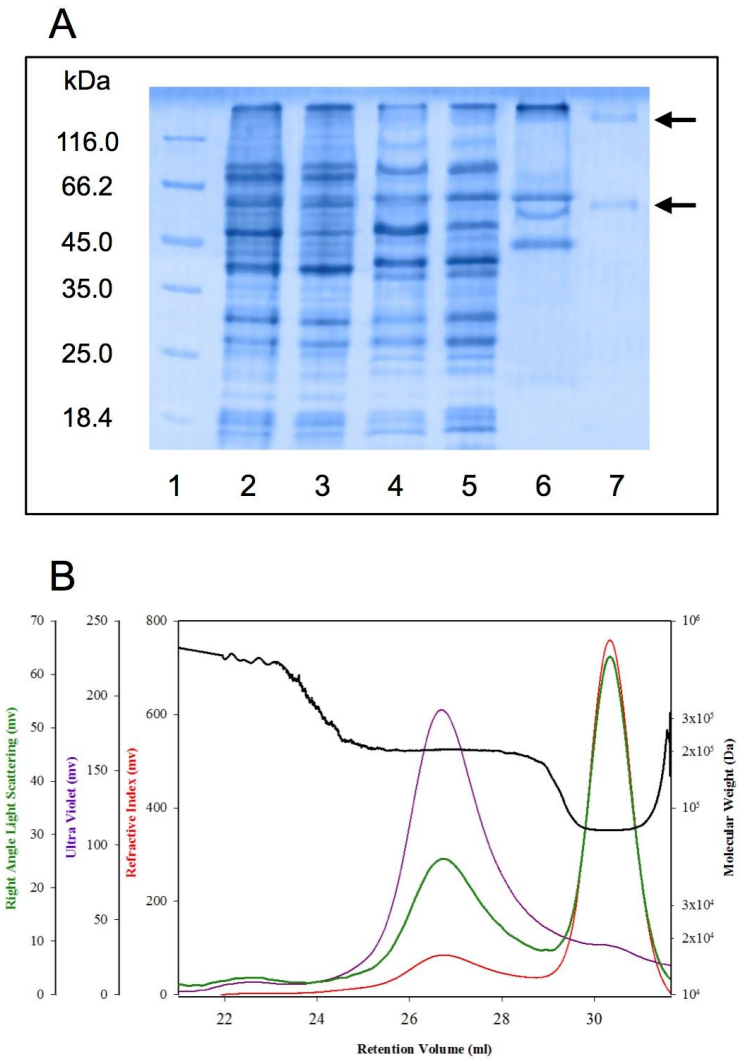

Fig. 1. Purification to homogeneity and multiangle light scattering (MALS) of IhOCC. (A) Proteins from each purification step was analyzed on 12% SDS-PAGE. (1) molecular weight markers, (2) membrane fraction, (3) solubilisate, (4) flow-through Q-Sepharose, (5) flow-through SP-Sepharose, (6) after Superdex 200, and (7) after hydroxyapatite. The arrows

indicate the monomeric and trimeric state of IhOCC. The presence of the trimeric state in the SDS-PAGE arises from the hyperthermophilic properties of the protein. (B) Chromatogram from a size exclusion experiment of IhOCC. Molecular weight calculated from MALS is presented in black, UV absorbance in purple, refractive index in red and RALS (right angle light scattering) in green.

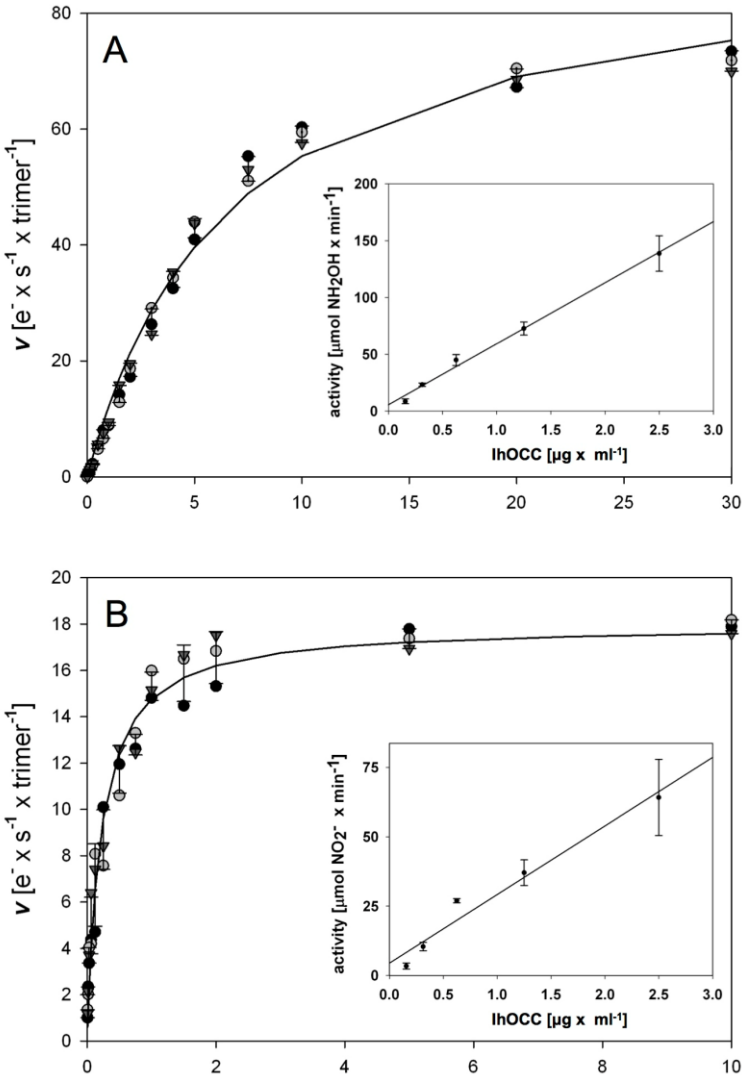

Fig. 2. Reactivity of IhOCC towards hydroxylamine (A) and nitrite (B). Enzyme activities were routinely determined at 80 °C under strictly anaerobic conditions in 50 mM K-phosphate pH 7.0. The solid lines through the data points are the fits to the Michaelis-Menten equation

using non-linear regression; insets show the dependence of hydroxylamine- and nitrite-reducing activity on the concentration 0.125 - 2.5 μg ml^{-1} of IhOCC.

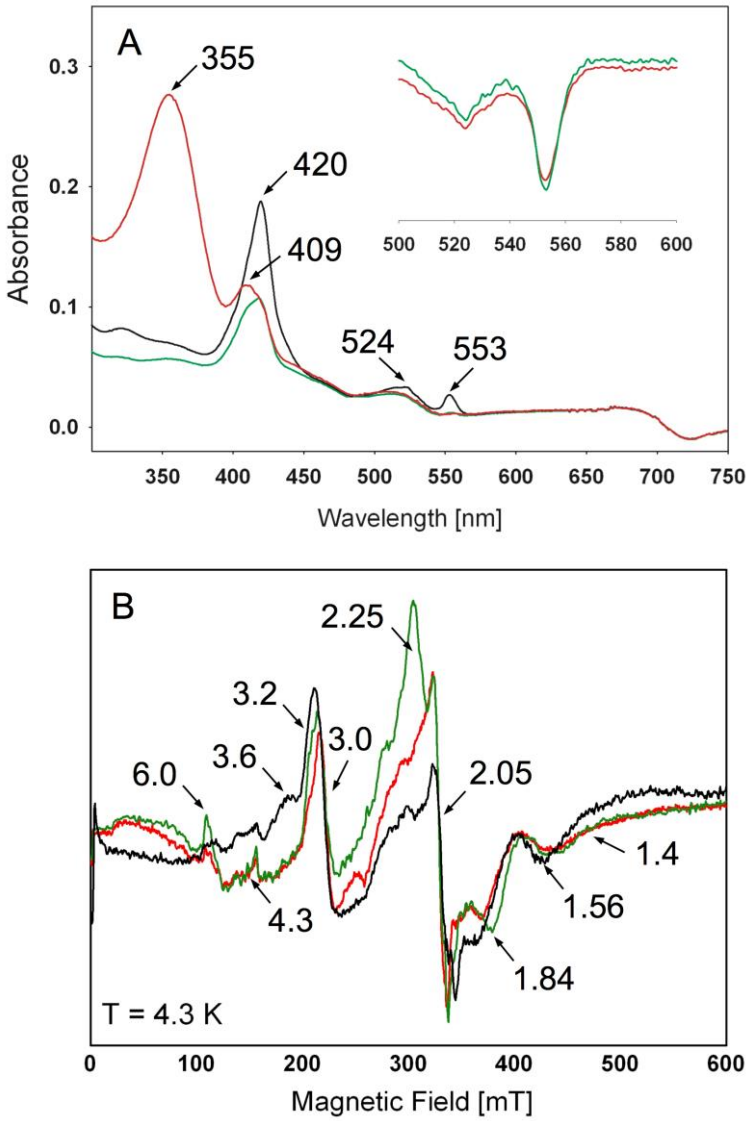

Fig. 3. UV/Vis and EPR spectra of IhOCC. (A) As purified (black) and with addition of either 20 mM nitrite (red) or hydroxylamine (green); inset shows enlargement of the (reduced minus oxidized) difference spectra around the α and β peaks. UV/Vis spectra were recorded in 50 mM K-phosphate pH 7.0 at 22 °C under anoxic conditions. (B) Enzyme as isolated in 50 mM K-phosphate pH 7.0 (black), and after addition of either 2 mM nitrite (red) or hydroxylamine (green); continuous-wave EPR spectra, perpendicular mode, were recorded at 9.4 GHz (X-

band) microwave frequency, 100 kHz modulation frequency, 4.0 G modulation amplitude, and 0.3 mW microwave power.

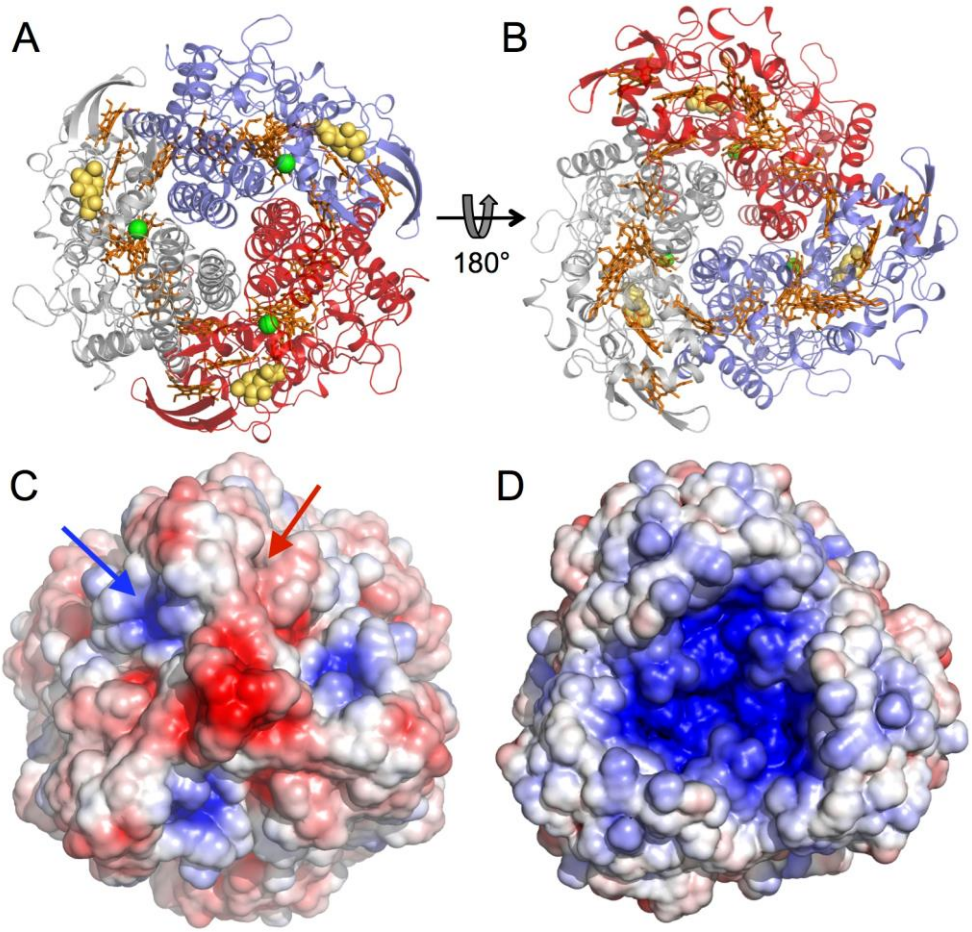

Fig. 4. Three dimensional structure of IhOCC from *I. hospitalis.* Each subunit is shown in a different colour (red, blue, gray). (A) represents the top and (B) the bottom view of IhOCC. Hemes represented in stick mode are coloured orange. The Ca^{2+} ion and N-acetylglucosamine (NAG) are shown as spheres in green and yellow, respectively. (C) and (D) are electrostatic potential surface maps of the corresponding top view and bottom view calculated by the program APBS at kT/e levels -5 and +5, respectively [52]. The arrows indicate the two channels presented in each protomer.

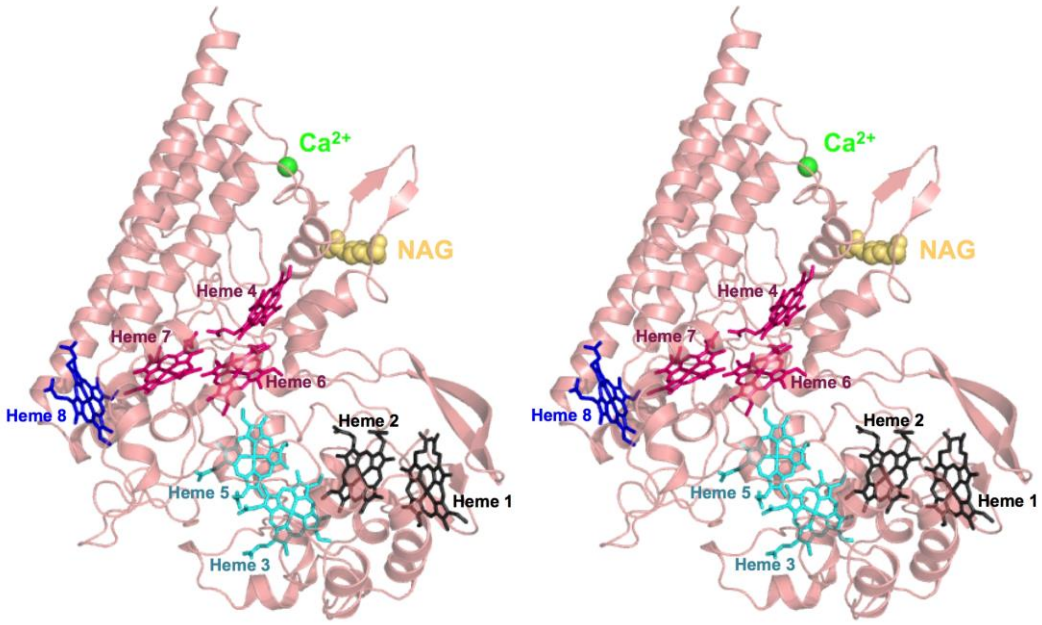

Fig. 5. Stereoview showing a single subunit of IhOCC. The diheme heme clusters I & II (cyan and black), the triple heme (pink) cluster and the single heme cluster (blue) are shown as stick models. The Ca^{2+} ion and NAG are represented as spheres in green and yellow, respectively.

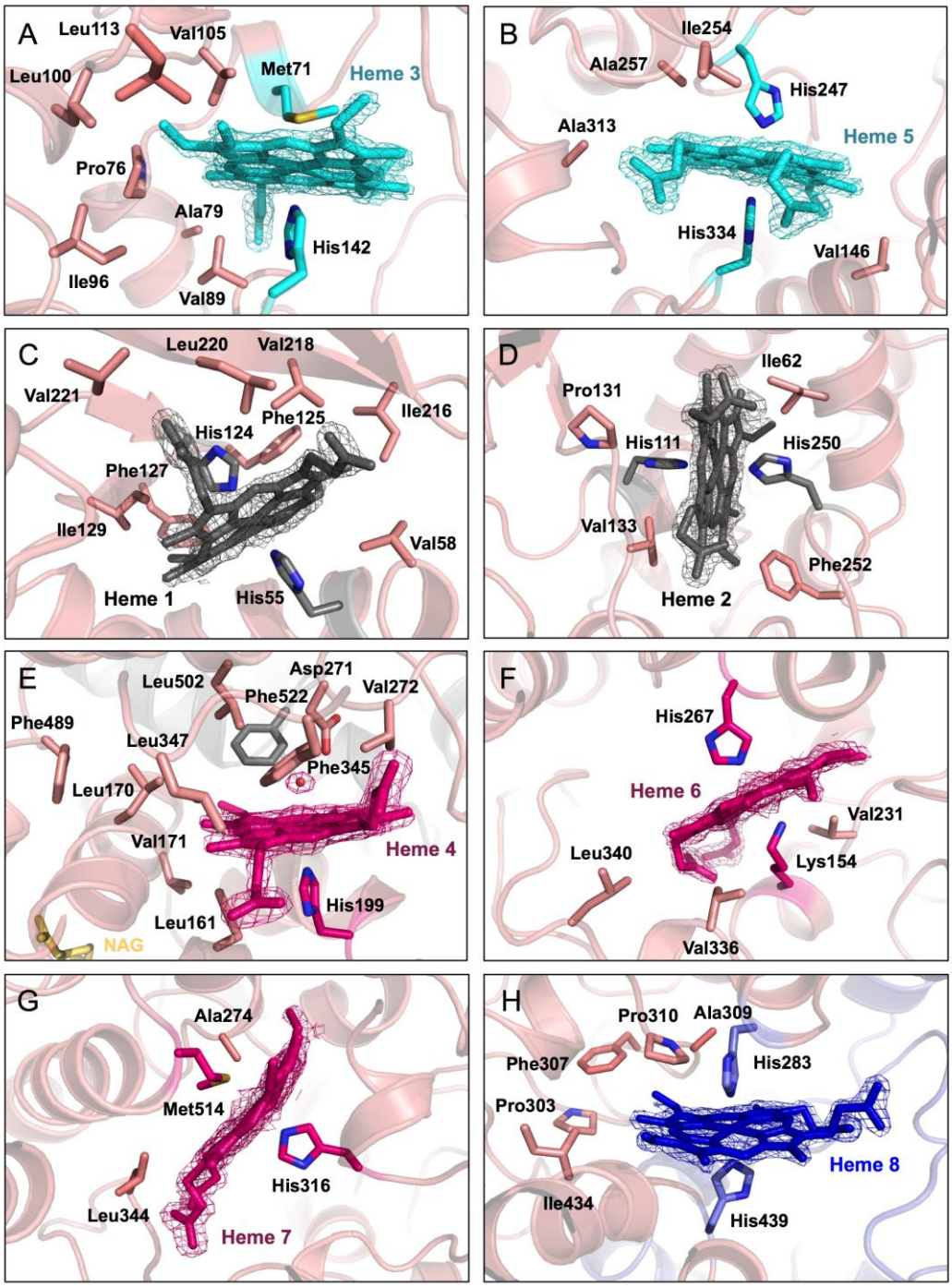

Fig. 6. Heme environment from a single subunit. The hydrophobic residues surrounding the hemes are shown in light red. The hemes and NAG are represented as stick model. The diheme heme cluster I includes heme 3 (A) and heme 5 (B) which are represented in cyan. The diheme heme cluster II includes heme 1 (C) and heme 2 (D) are illustrated in black. The triple heme cluster includes heme 4 (E), heme 6 (F) and heme 7 (G) are represented in pink. The single heme 8 (H) is shown in blue.

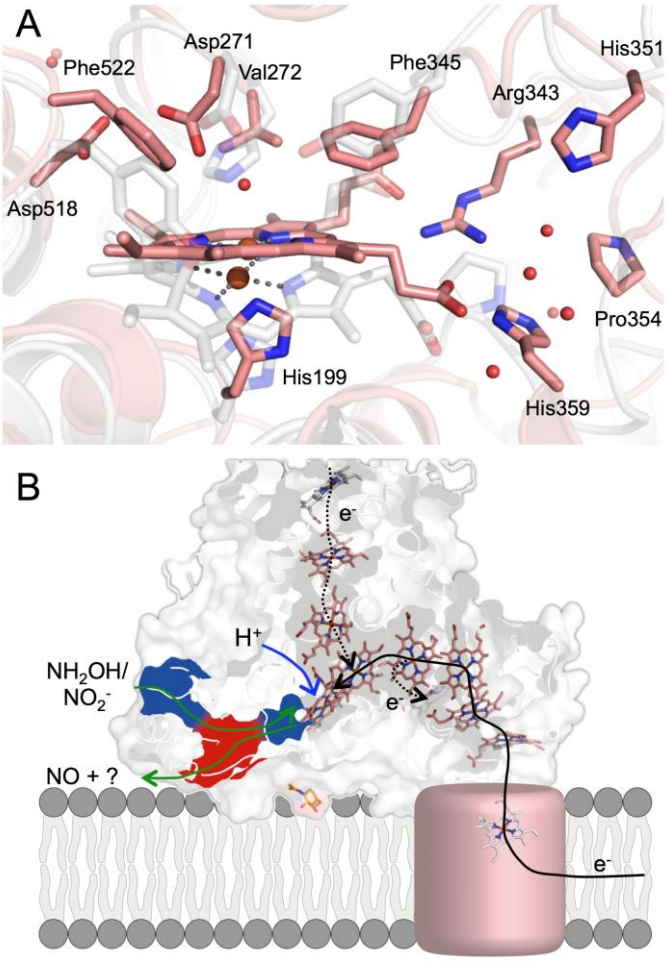

Fig. 7. Active site and proposed electron transfer pathway. (A) The active site of IhOCC is shown in light red and superposition of NeHAO is in light gray. Water molecules and iron atoms are represented in red and brown spheres, respectively. (B) Hemes, colored in light red and represented as stick models, belong to a single subunit while the grays colored hemes are located in the adjacent subunit and presumed interaction partner. The solid black line indicates the proposed major electron flow and the dashed black lines the electron flow through a proposed discriminator pathway [9]. The blue arrow indicates the proton transfer from the central funnel and the green arrows indicate the putative branched channel, respectively. The channels are colored with respect to their electrostatic surface potential. NAG is shown as stick model.

Table 1. Data collection and refinement statistics.

	Native	Fe peak 1.7 Å
Data collection		
Wavelength (Å)	1.0	1.7
Space group	R 3 2 :H	R 3 2 :H
Cell dimensions		
a, *b*, *c* (Å)	136.44, 136.44, 214.90	136.23, 136.23, 214.30
α□ □*β*□ □*γ*□ (°)	90, 90, 120	90, 90, 120
Resolution (Å)	43.73-1.70 (1.758-1.697)*	49.30-2.86
Total reflections	168637 (15991)	174864
Unique reflections	84428 (8058)	18012
R_{merged}	0.035 (0.39)	0.151
$I / \sigma(I)$	10.99 (1.62)	14.80
Completeness (%)	99.54 (95.97)	99.90
Redundancy	2.0 (2.0)	9.7
Refinement statistics		
Resolution (Å)	43.73-1.70 (1.758-1.697)*	
R_{work} / R_{free} (%)	0.1645/0.1994	
Wilson *B*-factor	21.10	
Av. *B-factor* (Å^2)	30.30	
No. Atoms	4824	
Protein	4054	
Ligands	359	
Water	411	
Bond-lengths deviation (Å)	0.010	
Bond-angles deviation (°)	1.52	
PDB code	4QO5	

*Values in parentheses are for highest-resolution shell.

Table 2. Heme ligands, binding cysteines and hydrophobic residues surrounding the corresponding hemes.

Heme cluster	Heme number	Heme axial ligands	Cys involved in thioether bonds	Hydrophobic residues around heme
Double heme cluster I	Heme 3	His142 & Met71	Cys138 & Cys141	Pro76, Ala79, Val89, Ile96, Leu100, Val105, Leu113
	Heme 5	His 247 & His334	Cys243 & Cys246	Val146, Ile254, Ala257, Ala313
Double heme cluster II	Heme 1	His55 & His124	Cys51 & Cys54	Val58, Phe125, Phe127, Ile 129, Ile216, Val218, Leu220, Val221
	Heme 2	His111 & His250	Cys107 & Cys110	Ile62, Pro131, Val133, Phe252
Triple heme cluster	Heme 4	His199 & HOH75	Cys198 & Cys195	Leu161, Leu170, Val171, Val272, Phe345, Leu347, Pro394, Phe489, Leu502
	Heme 6	His267& Lys154	Cys263 & Cys266	Val231, Val336, Leu340
	Heme 7	His316 & Met514	Cys312 & Cys315	Leu344, Ala274
Single heme	Heme 8	His283 & His439	Cys435 & Cys438	Phe307, Pro303, Pro310, Ile434, Ala309